Title

On the modeling of the intervertebral joint in multibody models for the spine

Journal

Multibody System Dynamics, 30(4)

ISSN

1384-5640

Authors

Christophy, Miguel
Curtin, Maurice
Faruk Senan, Nur Adila
et al.

Publication Date

2013-12-01

DOI

10.1007/s11044-012-9331-x

Peer reviewed

Multibody System Dynamics manuscript No.
(will be inserted by the editor)

On the modeling of the intervertebral joint in multibody models for the spine

Miguel Christophy · Maurice Curtin · Nur Adila Faruk Senan · Jeffrey C. Lotz · Oliver M. O'Reilly

Received: date / Accepted: date/

Abstract The need to develop feasible computational musculoskeletal models of the spine has led to the development of several multibody models. Central features in these works are models for the ligaments, muscles, and intervertebral joint. The purpose of the present paper is to show how experimental measurements of joint stiffnesses can be properly incorporated using a bushing element. The required refinements to existing bushing force functions in musculoskeletal software platforms are discussed and further implemented using a SpineBushing element specific to the intervertebral joint. Four simple lumbar spine models are then used to illustrate the accompanying improvements. Electronic supplemental material for this article includes a complementary review of formulations of stiffness matrices for the intervertebral joint.

Miguel Christophy · Nur Adila Faruk Senan · Oliver M. O'Reilly
Department of Mechanical Engineering,
University of California at Berkeley,
Berkeley, CA 94720-1740
USA
Tel.: +510-642-0877
Fax: +510-643-5599
E-mail: christophy@gmail.com
E-mail: adilapapaya@gmail.com
E-mail: oreilly@berkeley.edu

Maurice Curtin
School of Electrical, Electronic and Communications Engineering
University College Dublin
Belfield, Dublin 4,
Ireland
E-mail: moecurtin@gmail.com

Jeffrey C. Lotz
Department of Orthopaedic Surgery,
University of California at San Francisco,
San Francisco, CA 94143-0514
USA
Tel.: +415-476-7881
Fax.: +415-476-1128
E-mail: lotzj@orthosurg.ucsf.edu

Keywords Spinal kinematics · Musculoskeletal multibody models · Stiffness matrix · bushing element

1 Introduction

Recent medical and technological improvements have led to an increased demand for user-friendly, computationally inexpensive numerical models of the human body free of the ethical and logistical constraints imposed by experimental analyses. The existence of these models is anticipated to help pave the way for easy, cost effective, and comprehensive studies on the efficacies of different physical therapy options and the evaluation of prosthetic devices.

Unfortunately, the complexities surrounding the anatomy and function of the intervertebral joint present obstacles in simply, yet accurately, mimicking its properties in spinal models. Following the lead set by White and Panjabi [41], some researchers have assumed that the motion of each spinal vertebra can be written as a function of the net motion of the lumbar spine [3,17,40,44]. The suitability of this approach to studying true spinal motion however is questionable as there is a large amount of wide inter-subject variability [12]. The numerical cost of constraint functions is also a prohibitive factor especially for larger degree-of-freedom models. The stiffness matrix parameterization of the intervertebral joint presents a viable alternative.

Interestingly, Panjabi pioneered the use of a 6x6 stiffness matrix model for the intervertebral joint. Extrapolating upon theory initially developed as part of his thesis [26], he presented an elegant elucidation of its application to the joints of the spine in [25]. Three years later, [27] proposed a stiffness matrix K_P to model the joint (cf. Fig. 1). Assuming sagittal plane symmetry of the intervertebral joint and restricting attention to infinitesimal rotations, the number of stiffnesses in the matrix K_P were reduced from 36 to 12.[1]

Subsequent works by Gardner-Morse, Stokes and their coworkers [11,33,34,35] have measured the 12 parameters of K_P. However, over twenty years elapsed since Panjabi's initial work before detailed spinal models featuring a complete stiffness matrix were introduced. The first of these, presented in [30], used stiffness matrices obtained in [8]. Further refinements on this model have focused on improving muscle architecture and optimization routines for predicting muscle activation patterns [9,31,32,33]. Aside from the elegant study by [10] demonstrating the increase in intervertebral joint stiffness with increasing axial load, little mention has been made with regards to using newer data that capture the effects of preload and various experimental loading schemes on the ensuing stiffness matrix [15,24,28,36].

Concurrent with the aforementioned development of a stiffness matrix, advances in computational modeling have led to the development of software capable of creating and analyzing musculoskeletal models of the human body. Of these, software platforms such as the LifeMOD Biomechanics Modeler (MSC Software, Santa Ana, CA), visualNastran 4D (MSC Software, Santa Ana, CA), APOLLO [29], SIMM, and OpenSim [6], have adopted the bushing elements used in vehicle dynamics software [1,2,18] to model the properties of the intervertebral joint. These elements generate forces and moments between a pair of body segments equivalent to those that would be exerted by diagonal stiffness and damping matrices with zero resting length.

[1] An example of a stiffness matrix with the aforementioned symmetries can be seen in Eqn. (24) below.

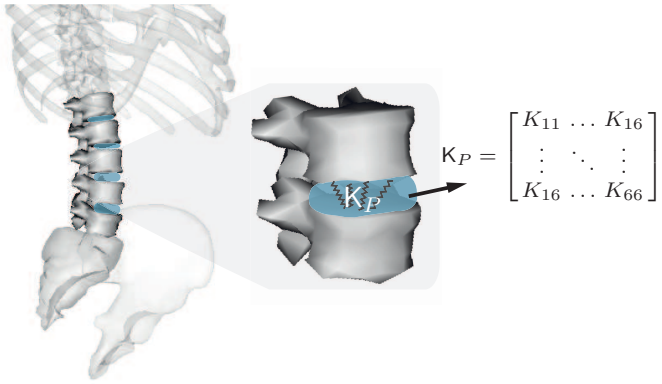

Fig. 1: *Schematic of the intervertebral joint as a symmetric* 6×6 *stiffness matrix,* K_P *as first proposed by [25]. The elements of* K_P *are initially determined from load-displacement experiments performed on vertebral pairs.*

The approximate similarity between the bushing element and the intervertebral joint has led to its increased use in musculoskeletal models of the spine (see [7,14,16,19,20,21,23]). Here, we describe in further detail the application of the bushing element to model the intervertebral joint and clarify some common misconceptions. We elaborate on the subtleties of the bushing element, some of which can lead to erroneous bushing forces and moments if not applied correctly. For instance, if the bushing frames are not initially coincident with each other, large forces and moments ensue. Placing the frames coincident eliminates this, but introduces an artificial moment unless certain, non-trivial modifications are made. In addition, the diagonal nature of the typical bushing element used in musculoskeletal models of the spine fails to replicate the coupled motion that is a defining feature of the intervertebral joint. Consequently, possibly erroneous kinematics, reaction forces, and computed muscle forces can be produced by the bushing element.

To overcome these complications, we created a SpineBushing element in OpenSim, an open-source musculoskeletal software platform [6]. This element has two key features that makes it suitable for modeling the intervertebral joints of the spine. First, the *change* in relative motion between the bushing frames is used to compute the resulting forces and moments. This is analogous to modifying the bushing element from a stiffness matrix with zero resting length, to a stiffness matrix with resting length equal to the distance between the centers of mass of the adjacent vertebral bodies in the neutral posture. In addition, our SpineBushing element incorporates arbitrary 6×6 stiffness matrices and thus permits the analysis of coupling between the different degrees of freedom and this is illustrated in the present paper through a series of models for the lumbar spine.

We presume a familiarity with rigid body dynamics and Euler angle parameterizations of rotations in the main text. For readers unfamiliar with this background or our notation, a supplementary online resource is provided. Section 1 of this resource discusses parameterizations of rigid body motions, followed by background on the 1-2-3 set of Euler angles and the relative motion of a pair of rigid bodies in Sections 2 and 3 respectively. Section 6 of this resource contains additional discussion on the stiffness

matrix K_P and its relationship to other stiffness matrices that have appeared in the recent literature.

In the present paper, arrays of real numbers are denoted by san-serif Roman letters, such as T, p, while vectors and tensors are denoted by bold-faced Roman letters, e.g., $\bar{\mathbf{x}}$ and $\mathbf{R}$. Additionally, we reserve capital letter sub- and super-scripts to indicate specific bodies (e.g., bodies $\mathcal{V}_K$, basis vectors $\mathbf{e}_i^K$) while uncapitalized indices are used to specify components of vectors, tensors, arrays of real numbers and matrices, such as ω_i, K_{ij}, q_i, $\tilde{T}_{ij}$.

There is a considerable diversity in the choices of coordinate axes and Euler angles used in the spinal mechanics literature. In this paper, will use a 1-2-3 set of Euler to parameterize the relative rotation tensor $\mathbf{R}$ between a pair of vertebra, and let the basis vectors $\left\{\mathbf{e}_1^K, \mathbf{e}_3^K, \mathbf{e}_3^K\right\}$ point anterior, superior, and to the right, respectively (cf. Fig 2). As a result, we have the following correspondences for the three Euler angles β_1, β_2, and β_3:

$$\begin{gathered}\beta_1 \equiv \text{lateral bending,}\\ \beta_2 \equiv \text{axial rotation,}\\ \beta_3 \equiv \text{flexion-extension with } \beta_3 > 0 \text{ corresponding to extension.}\end{gathered}$$

We emphasize that these angles of rotation pertain to the rotation of a body $\mathcal{V}_2$ relative to a body $\mathcal{V}_1$. Further details on Euler angle representations can be found in Section 3 of the Online Resource.

A number of different stiffness matrices associated with the intervertebral joint are examined. The first is the stiffness matrix K^E determined experimentally from infinitesimal uniaxial motion. We will assume that K^E is symmetric. Further details on this approximation are given in Sections 4, 5, and 6 of the Online Resource. The second stiffness matrix, K^B, is used to denote the stiffness matrix of the bushing element detailed in Section 3 while K^S, the third stiffness matrix, is used for the stiffness matrix employed in the SpineBushing element. We note that K^S will be prescribed using experimental data: $\mathsf{K}^S = \mathsf{K}^E$.

2 The experimental stiffness matrix K^E

The stiffness matrix and bushing element are both used to relate the relative motion between two rigid bodies to the resulting forces and moments acting at specified points on each of the individual bodies. However, there are a number of distinct differences between the standard stiffness matrix K^E obtained experimentally and the stiffness matrix K^B featured in typical bushing elements. The two main differences relates to the zero resting length of the bushing element and the points about which the forces and moments are applied. Prior to elaborating upon this however, it is appropriate to first describe how the intervertebral joint stiffness matrix elements are determined experimentally.

Most commonly, the lower vertebra is fixed, the upper vertebra subjected to an infinitesimal motion, and the forces and moments due to the ensuing deformation measured [10,11,34,35]. Alternatively, a force or moment is applied and the resulting deformations measured [4,27] (Fig. 3). Variations of these protocols have also been tested using larger deformations [24].

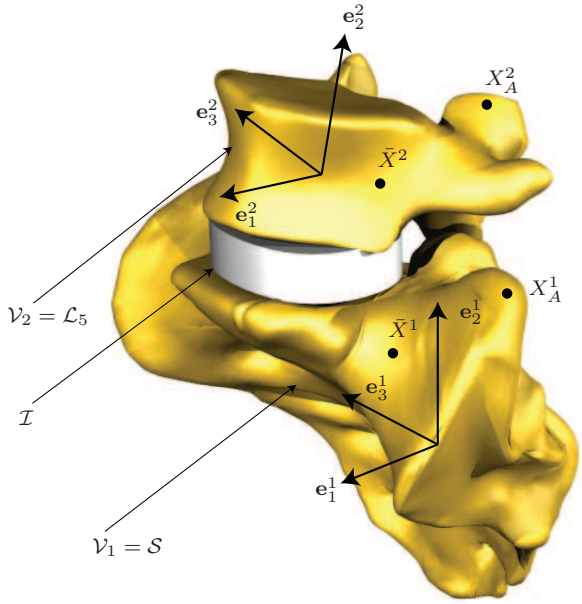

Fig. 2: *An example of a vertebral motion segment consisting of the sacrum $\mathcal{S}$, the fifth lumbar vertebra $\mathcal{L}_5$ and the intervertebral disc $\mathcal{I}$. The basis vectors $\left\{\mathbf{e}_1^1, \mathbf{e}_3^1, \mathbf{e}_3^1\right\}$ and $\left\{\mathbf{e}_1^2, \mathbf{e}_3^2, \mathbf{e}_3^2\right\}$ are attached to the bodies $\mathcal{S}$ and $\mathcal{L}_5$, respectively. The position vectors of the centers of mass $\bar{X}^1$ and $\bar{X}^2$ are denoted by $\bar{\mathbf{x}}^1$ and $\bar{\mathbf{x}}^2$ respectively. The location of potential landmarks X_A^1 on $\mathcal{S}$ and X_A^2 on $\mathcal{L}_5$ are also shown.*

To elaborate, we define the relative translation between the landmark points X_A^1 and X_A^2 using a displacement vector $\mathbf{y}_A$,

$$\mathbf{y}_A = \mathbf{x}_A^2 - \mathbf{x}_A^1 = \sum_{i=1}^{3} Y_i \mathbf{E}_i = \sum_{k=1}^{3} = y_k^1 \mathbf{e}_k^1, \tag{1}$$

and use the rotation tensor $\mathbf{R}$,

$$\mathbf{R} = \mathbf{R}\left(\beta_1, \beta_2, \beta_3, \tilde{\mathbf{g}}_1, \tilde{\mathbf{g}}_2, \tilde{\mathbf{g}}_3\right), \tag{2}$$

to characterize the relative rotation between the bodies. Here, β_k denote the Euler angles used to parameterize $\mathbf{R}$ and $\{\tilde{\mathbf{g}}_1, \tilde{\mathbf{g}}_2, \tilde{\mathbf{g}}_3\}$ are the set of Euler basis vectors. Note that the Euler basis vectors are not necessarily the same as the body-fixed basis vectors $\left\{\mathbf{e}_1^K, \mathbf{e}_2^K, \mathbf{e}_3^K\right\}$. As mentioned in Section 3 of the Online Resource, the Euler basis is orthogonal to the dual Euler basis $\left\{\tilde{\mathbf{g}}^1, \tilde{\mathbf{g}}^2, \tilde{\mathbf{g}}^3\right\}$:

$$\tilde{\mathbf{g}}_i \cdot \tilde{\mathbf{g}}^j = \delta_i^j. \tag{3}$$

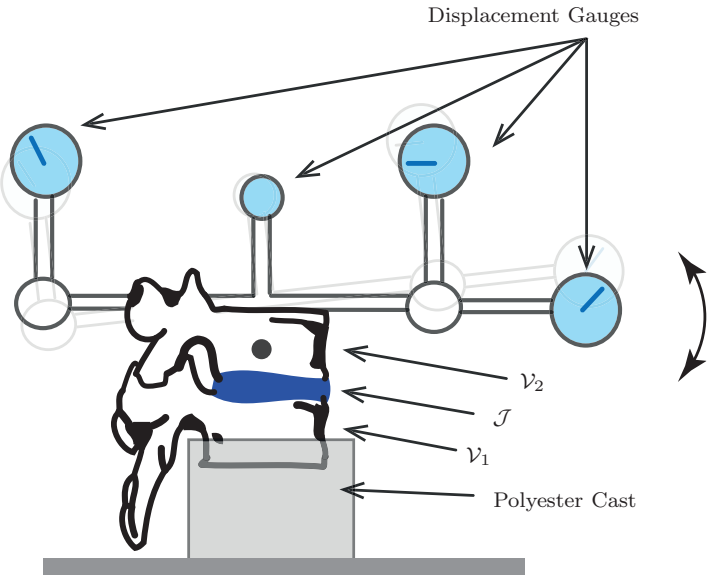

Fig. 3: *Schematic of the stiffness matrix testing apparatus used in Panjabi et al.'s seminal paper [27]. The lower vertebra, $\mathcal{V}_1$ was fixed by bolting it to a polyester cast. Load vector components, one at a time, were then applied to the upper vertebra $\mathcal{V}_2$ via a threaded pin and the displacements measured using three displacement gauges. The elements of the experimental stiffness matrix K^E used to model the intervertebral joint $\mathcal{J}$ were computed from the resulting load-displacement curves.*

We can now define the generalized displacement and force arrays:

$$\Delta \mathsf{y}_A = \begin{bmatrix} \Delta \mathbf{y}_A \cdot \mathbf{e}_1^1 \\ \Delta \mathbf{y}_A \cdot \mathbf{e}_2^1 \\ \Delta \mathbf{y}_A \cdot \mathbf{e}_3^1 \\ \Delta \boldsymbol{\beta} \cdot \tilde{\mathbf{g}}^1 \\ \Delta \boldsymbol{\beta} \cdot \tilde{\mathbf{g}}^2 \\ \Delta \boldsymbol{\beta} \cdot \tilde{\mathbf{g}}^3 \end{bmatrix}, \qquad \Delta \mathsf{F}_K^A = \begin{bmatrix} \left(\left(\mathbf{F}_K^A \right)' - \mathbf{F}_K^A \right) \cdot \mathbf{e}_1^1 \\ \left(\left(\mathbf{F}_K^A \right)' - \mathbf{F}_K^A \right) \cdot \mathbf{e}_2^1 \\ \left(\left(\mathbf{F}_K^A \right)' - \mathbf{F}_K^A \right) \cdot \mathbf{e}_3^1 \\ \left(\left(\mathbf{M}_K^A \right)' - \mathbf{M}_K^A \right) \cdot \tilde{\mathbf{g}}_1 \\ \left(\left(\mathbf{M}_K^A \right)' - \mathbf{M}_K^A \right) \cdot \tilde{\mathbf{g}}_2 \\ \left(\left(\mathbf{M}_K^A \right)' - \mathbf{M}_K^A \right) \cdot \tilde{\mathbf{g}}_3 \end{bmatrix}. \tag{4}$$

Here, $\Delta \mathsf{F}_K^A$ corresponds to the change in generalized force acting on the landmark point X_A^2 on the upper body and $\Delta \mathsf{y}_A$ denotes the increments to the generalized relative displacement between a landmark point X_A^2 on the upper vertebra relative to a landmark point X_A^1 on the lower vertebra. That is, $\Delta \mathsf{y}_A$ is composed of the components of the increment in displacement vector $\mathbf{y}_A$ and increments in the Euler

angles:[2]

$$\Delta y_k^1 = \Delta \mathbf{y}_A \cdot \mathbf{e}_k^1, \qquad \Delta \beta_k = \Delta \boldsymbol{\beta} \cdot \tilde{\mathbf{g}}^k, \qquad (k = 1, 2, 3). \tag{5}$$

The elements of the experimental stiffness matrix K^E can then be determined by comparing the changes in the forces and moments to the relative motion between the upper and lower vertebra.

$$\Delta \mathsf{F}_2^A = -\Delta \mathsf{F}_1^A = -\mathsf{K}^E \Delta \mathsf{y}_A. \tag{6}$$

The equal and opposite nature of the generalized forces should be noted.

One of the more common choices of the landmark points X_A^K are the vertebral centers of geometry but one can also opt to use other landmarks such as points on the upper and lower vertebral surfaces [4,11,27,34,35]. Note that, if these, or other, experimental data are used to populate bushing stiffness matrices it is crucial to identify the landmark material points X_A^1 and X_A^2 associated with the relative displacement $\mathbf{y}_A$ and to accommodate any possible differences in the choices of Euler angles and basis vectors.

Further details with regards to the derivation of the stiffness matrix parameterization of the intervertebral joint can be found in Sections 4-6 of the Online Resource.

3 The bushing element for the OpenSim musculoskeletal software platform

The bushing element commonly used in musculoskeletal software platforms computes the forces and moments proportional to the relative motions of two frames. This element is identical in function to applying a diagonal stiffness and damping matrix between the frames. Here, we elaborate on the algorithm behind the bushing element, and show how it can be used to accommodate a stiffness matrix. We base our analysis on the bushing force function available in OpenSim as it is an open-source software platform with readily accessible documentation.

3.1 Kinematical preliminaries

Following the development of bushing elements in the literature [1,2,18], it is necessary to introduce several sets of frames. The first of these sets are the two body frames $\mathbb{F}_1$ and $\mathbb{F}_2$ situated at the centers of mass of the vertebral bodies $\mathcal{V}_1$ and $\mathcal{V}_2$:

$$\mathbb{F}_1 = \left\{ \bar{\mathbf{x}}^1, \left\{ \mathbf{e}_1^1, \mathbf{e}_2^1, \mathbf{e}_3^1 \right\} \right\}, \qquad \mathbb{F}_2 = \left\{ \bar{\mathbf{x}}^2, \left\{ \mathbf{e}_1^2, \mathbf{e}_2^2, \mathbf{e}_3^2 \right\} \right\}. \tag{7}$$

The second set of frames correspond to the joint frames:

$$\mathbb{J}_1 = \left\{ \mathbf{x}_J^1, \left\{ \mathbf{j}_1^1, \mathbf{j}_2^1, \mathbf{j}_3^1 \right\} \right\}, \qquad \mathbb{J}_2 = \left\{ \mathbf{x}_J^2, \left\{ \mathbf{j}_1^2, \mathbf{j}_2^2, \mathbf{j}_3^2 \right\} \right\}. \tag{8}$$

As the joint frames $\mathbb{J}_1$ and $\mathbb{J}_2$ are used to characterize the motion of $\mathcal{V}_2$ relative to $\mathcal{V}_1$, they are coincident in the neutral position:

$$\mathbf{x}_J^1 = \mathbf{x}_J^2, \qquad \mathbf{j}_i^1 = \mathbf{j}_i^2, \qquad (k = 1, 2, 3). \tag{9}$$

[2] The reader is also referred to Section 5.1 of the Online Resource for further details on the specifications of $\Delta \mathbf{y}_A$ and $\Delta \boldsymbol{\beta}$.

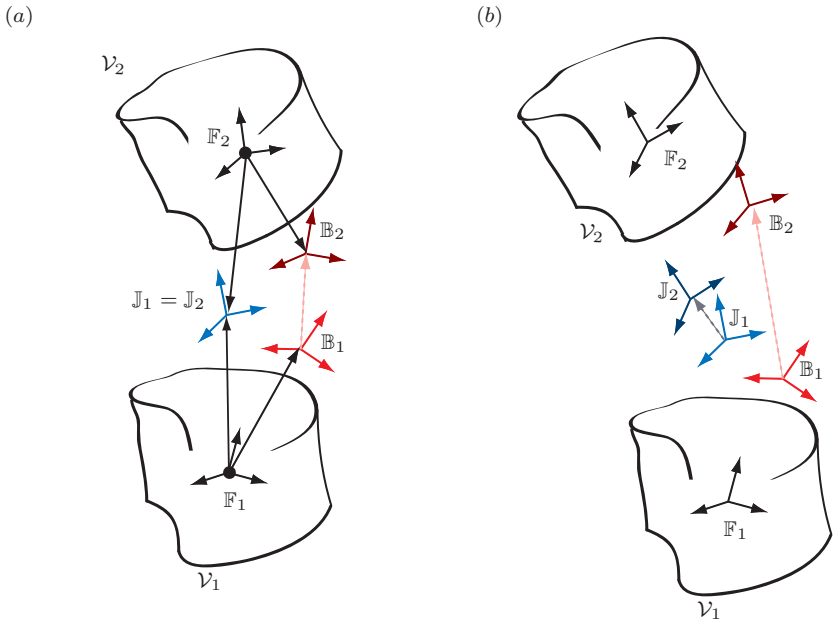

Fig. 4: *The frames associated with the bushing element. (a) The frames in the neutral position, and (b) the frames in a displaced position. Once specified, the relative orientation between the frames* $\mathbb{F}_K$, $\mathbb{J}_K$, *and* $\mathbb{B}_K$ *remain fixed.*

but deviate from each other as the bodies move. The third set of frames are known as the bushing frames and are associated with the lower and upper vertebra $\mathcal{V}_1$ and $\mathcal{V}_2$, respectively:

$$\mathbb{B}_1 = \left\{\mathbf{x}_B^1, \left\{\mathbf{b}_1^1, \mathbf{b}_2^1, \mathbf{b}_3^1\right\}\right\}, \qquad \mathbb{B}_2 = \left\{\mathbf{x}_B^2, \left\{\mathbf{b}_1^2, \mathbf{b}_2^2, \mathbf{b}_3^2\right\}\right\}. \tag{10}$$

The six frames are depicted in Fig. 4. It is important to note that $\mathbf{j}_i^1$ and $\mathbf{b}_i^1$ corotate with the first vertebral body $\mathcal{V}_1$ and $\mathbf{j}_i^2$ and $\mathbf{b}_i^2$ corotate with the second vertebral body $\mathcal{V}_2$.

In addition to the rotation tensors $\mathbf{Q}_1$ and $\mathbf{Q}_2$ associated with the respective frames $\mathbb{F}_1$ and $\mathbb{F}_2$, several additional rotation tensors must be defined. For example, the rotation tensor $\mathbf{Q}_1^B$ associated with the frame $\mathbb{B}_1$ has the representation

$$\mathbf{Q}_1^B = \mathbf{b}_1^1 \otimes \mathbf{E}_1 + \mathbf{b}_2^1 \otimes \mathbf{E}_2 + \mathbf{b}_3^1 \otimes \mathbf{E}_3. \tag{11}$$

Because the basis vectors $\left\{\mathbf{b}_1^1, \mathbf{b}_2^1, \mathbf{b}_3^1\right\}$ corotate with $\mathcal{V}_1$, it can be shown that $\mathbf{Q}_1$ and $\mathbf{Q}_1^B$ are related:

$$\mathbf{Q}_1 = \mathbf{T}_1^B \mathbf{Q}_1^B \tag{12}$$

where $\mathbf{T}_1^B$ is a rotation tensor: $\mathbf{e}_i^1 = \mathbf{T}_1^B \mathbf{b}_i^1$. Hence,

$$\mathbf{R} = \mathbf{Q}_2 \mathbf{Q}_1^T = \mathbf{T}_2^B \mathbf{Q}_2^B \left(\mathbf{T}_1^B \mathbf{Q}_1^B\right)^T, \qquad \mathbf{R}^B = \mathbf{Q}_2^B \left(\mathbf{Q}_1^B\right)^T. \tag{13}$$

When the three frames $\mathbb{F}_K$, $\mathbb{J}_K$ and $\mathbb{B}_K$ are aligned, $\mathbf{Q}_K^B = \mathbf{Q}_K$ and $\mathbf{R} = \mathbf{R}^B$.

Following (1) and (2), we define the relative position between the bushing frames using the relative position vector

$$\mathbf{y}_B = \mathbf{x}_B^2 - \mathbf{x}_B^1, \tag{14}$$

and use the set of Euler angles $\{\beta_{B,1}, \beta_{B,2}, \beta_{B,3}\}$ to parameterize $\mathbf{R}^B$:

$$\mathbf{R}^B = \mathbf{R}^B\left(\beta_{B,1}, \beta_{B,2}, \beta_{B,3}, \tilde{\mathbf{g}}_{B,1}, \tilde{\mathbf{g}}_{B,2}, \tilde{\mathbf{g}}_{B,3}\right). \tag{15}$$

In the sequel, we employ the vector $\boldsymbol{\beta}_B = \sum_{k=1}^{3} \beta_{B,k}\tilde{\mathbf{g}}_{B,k}$. This vector is analogous to the infinitesimal rotation vector $\Delta\boldsymbol{\beta}$.

Unlike the joint frames $\mathbb{J}_1$ and $\mathbb{J}_2$, the bushing frames $\mathbb{B}_1$ and $\mathbb{B}_2$ need not be coincident in the neutral position:

$$\mathbf{y}_B \neq \mathbf{0}, \qquad \mathbf{R}^B \neq \mathbf{I}. \tag{16}$$

It will shortly become apparent that, due to the manner with which the bushing force is computed, non-zero bushing forces will be exerted on the pair of bodies if (16) holds.

3.2 The bushing forces and moments

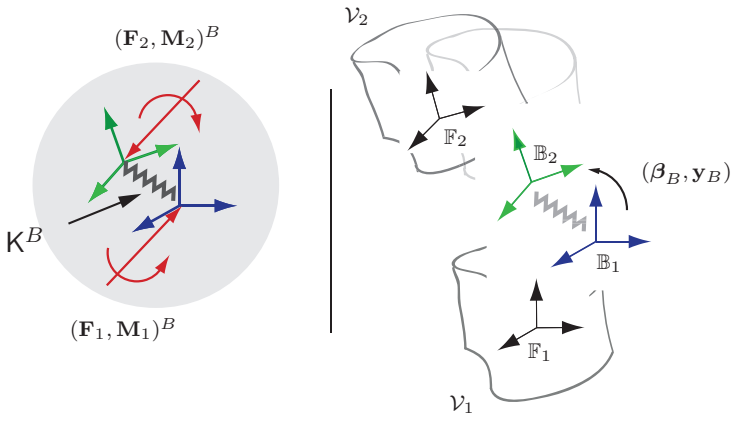

Fig. 5: *Schematic of the bushing element computations for a $\mathcal{V}_1$-$\mathcal{V}_2$ motion segment. The forces and moments due to the bushing element - exerted at the frames $\mathbb{B}_1$ and $\mathbb{B}_2$ shown on the right - are related to the relative motion $(\mathbf{y}_B, \boldsymbol{\beta}_B)$ between the two bushing frames using the bushing stiffness matrix K^B by (18).*

It is convenient to first define the following arrays:

$$\mathsf{y}_B = \begin{bmatrix} \mathbf{y}_B \cdot \mathbf{b}_1^1 \\ \mathbf{y}_B \cdot \mathbf{b}_2^1 \\ \mathbf{y}_B \cdot \mathbf{b}_3^1 \\ \beta_{B,1} = \boldsymbol{\beta}_B \cdot \tilde{\mathbf{g}}_B^1 \\ \beta_{B,2} = \boldsymbol{\beta}_B \cdot \tilde{\mathbf{g}}_B^2 \\ \beta_{B,3} = \boldsymbol{\beta}_B \cdot \tilde{\mathbf{g}}_B^3 \end{bmatrix}, \qquad \mathsf{F}_K^B = \begin{bmatrix} \mathbf{F}_K^B \cdot \mathbf{b}_1^1 \\ \mathbf{F}_K^B \cdot \mathbf{b}_2^1 \\ \mathbf{F}_K^B \cdot \mathbf{b}_3^1 \\ \mathbf{M}_K^B \cdot \tilde{\mathbf{g}}_{B,1} \\ \mathbf{M}_K^B \cdot \tilde{\mathbf{g}}_{B,2} \\ \mathbf{M}_K^B \cdot \tilde{\mathbf{g}}_{B,3} \end{bmatrix}, \tag{17}$$

where $\mathbf{F}_K^B$ and $\mathbf{M}_K^B$ indicate the force and moment vectors exerted by the bushing element on the respective bushing frames $\mathbb{B}_K$. The generalized relative displacement array y^B is then used in combination with the stiffness matrix K^B to determine the bushing forces and moments acting on the two bushing frames:[3]

$$\mathsf{F}_2^B = -\mathsf{K}^B \mathsf{y}_B, \qquad \mathsf{F}_1^B = -\mathsf{F}_2^B. \tag{18}$$

This is illustrated in Fig. 5. The generalized forces F_1^B and F_2^B in (18) have force components expressed in the frame $\{\mathbf{b}_1^1, \mathbf{b}_2^1, \mathbf{b}_3^1\}$ fixed to $\mathcal{V}_1$ and moments expressed in the dual Euler basis associated with the relative rotation tensor $\mathbf{R}^B$ (cf. (17) and (18)).

Notice that the relative displacement and orientation between the bushing frames is used as opposed to the *change* in relative position and orientation. Conceptually, this is similar to a spring with a zero resting length. Consequently, F_2^B and F_1^B are non-zero in the neutral position if the bushing frames are not initially coincident (Fig. 6).

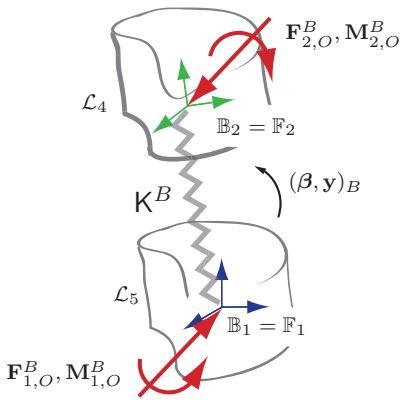

Fig. 6: *Schematic showing the case where bushing frames $\mathbb{B}_K$ are placed coincident with the body frames $\mathbb{F}_K$ resulting in non-zero forces and moments in the neutral posture, denoted using the subscript O (cf. (18) and (19)).*

3.3 Comments on experimental data

A number of notable differences exist between the forces and moments exerted by the bushing element and the experimental stiffness matrix associated with the intervertebral disc. If a set of stiffness data for K^E, such as those found in [11] or [27], are

[3] In OpenSim, the generalized force due to the bushing element $\mathsf{F}_1^B = -\mathsf{F}_2^B$ is exerted on the bushing frame $\mathbb{B}_2$ and an additional transformation applied to account for the shift from $\mathbb{B}_2$ to $\mathbb{B}_1$. Consequently, the generalized force acting on the frame $\mathbb{B}_1$ is *not* equal and opposite to that exerted on the frame $\mathbb{B}_2$ by the bushing element. Rather, the force and moment vectors exerted on $\mathbb{B}_1$ by the bushing element are given by

$$\mathbf{F}_1^B = -\mathbf{F}_2^B, \qquad \mathbf{M}_1^B = -\mathbf{M}_2^B + (\mathbf{x}_B^2 - \mathbf{x}_B^1) \times \mathbf{F}_B^1.$$

We will refrain from using this convention.

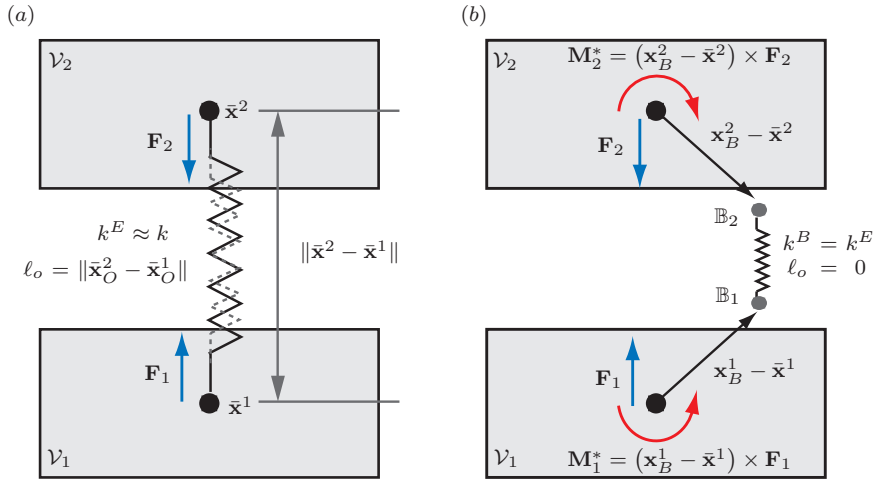

Fig. 7: *A simple two-dimensional example illustrating the importance of using the correct parameters in computing the bushing force. In (a), a spring with stiffness k and resting length ℓ_o is used to connect the two blocks $\mathcal{V}_1$ and $\mathcal{V}_2$. The forces exerted by the spring on the geometric centers of the two bodies are measured and the relationship between these forces and motion of the geometric centers are used to determine the spring constant $k^E \approx k$. The constant k^E is then (incorrectly) used in a model consisting of the two bodies connected by a bushing element with resting length $\ell_o = 0$ (b). This results in the spurious moments $\mathbf{M}^*_1$ and $\mathbf{M}^*_2$ about the geometric centers of the two bodies as detailed in the text.*

being used to prescribe the components of K^B, then the bushing frames $\mathbb{B}_1$ and $\mathbb{B}_2$ need to be placed coincident with the landmark points X^1_A and X^2_A used to determine the elements of K^E.[4] This ensures that the bushing forces exerted are consistent with the experimental forces used to measure K^E. Unfortunately, this introduces a non-zero force in the neutral posture equal to

$$\mathsf{F}^B_{2,O} = -\mathsf{F}^B_{1,O} = -\mathsf{K}^B \mathsf{y}_{B,O}, \tag{19}$$

where $\mathsf{F}^B_{2,O}$ and $\mathsf{F}^B_{1,O}$ are the generalized bushing forces acting at the centers of mass of the upper and lower vertebra respectively, $\mathsf{y}_{B,O}$ is the generalized displacement array between the bushing frames, and the subscript O is used to denote the neutral posture (cf. Fig. 6).

To eliminate the erroneous generalized forces (19), one could place the bushing frames initially coincident with each other since this guarantees $\mathsf{y}_B = \Delta\mathsf{y}_B$. However, this can introduce spurious moments at the vertebral centers once the frames begin to deviate. To elaborate consider the simple planar example shown in Fig. 7. Here, the bodies are connected by a spring whose line of action passes through the geometric centers. The spring has a stiffness, k and a resting length ℓ_o:

$$\ell_o = \|\bar{\mathbf{x}}^2_O - \bar{\mathbf{x}}^1_O\|. \tag{20}$$

[4] Recall that in both of these studies, the motion and loads at the vertebral centers of geometry ($\approx$ vertebral center of mass) were used to determine the elements of K^E.

The relationship between the spring force and the motion of the two bodies from the neutral posture are used to compute the experimental stiffness $k^E \approx k$. The same system is now connected by a bushing element with stiffness $k^B = k^E$, and zero resting length. As $\ell_o = 0$, placing the bushing frames $\mathbb{B}_1$ and $\mathbb{B}_2$ at $\bar{\mathbf{x}}^1$ and $\bar{\mathbf{x}}^2$ respectively result in a residual force in the neutral posture. To overcome this, the bushing frames are typically placed coincident with each other initially. However, this results in the additional spurious moments $\mathbf{M}_1^*$ and $\mathbf{M}_2^*$ about the centers of geometry of both bodies when the bushing frames are no longer coincident:

$$\mathbf{M}_1^* = \left(\mathbf{x}_B^1 - \bar{\mathbf{x}}^1\right) \times \mathbf{F}_1, \qquad \mathbf{M}_2^* = \left(\mathbf{x}_B^2 - \bar{\mathbf{x}}^2\right) \times \mathbf{F}_2. \tag{21}$$

4 A SpineBushingElement function for the OpenSim Platform

As can be inferred from the discussion in the previous section, the simplest method of ensuring compatibility with experimental measurements is to amend the existing bushing function such that the *change* in relative motion (from the neutral posture) is used to compute the ensuing bushing forces. One is then free to place the bushing frames at the landmark points $\mathbf{x}_A^1$ and $\mathbf{x}_A^2$ used to determine the elements of K^E. In this section, we discuss the development of a SpineBushing element that features this adjustment. Specifically, the SpineBushing forces and moments are computed using the change in relative motion between the SpineBushing frames. One of the integral arguments for utilizing the stiffness matrix parameterization lies in the straightforward manner with which the off-diagonal terms can be used to relate the coupling between the motion and loads along all six degrees-of-freedom of a spinal motion segment. And so, this simple, yet significant, modification is further supplemented with the ability to incorporate stiffness matrices with off-diagonal components.

With the aforementioned changes in place, we write the generalized force exerted at the SpineBushing frame $\mathbb{S}_2$ on the upper vertebra as

$$\mathsf{F}_2^S = -\mathsf{K}^S \Delta \mathsf{y}_S \tag{22}$$

where the super and subscript S has been used to associate the variables with the SpineBushing function. In (22), $\mathsf{K}^S = \mathsf{K}^E$, $\Delta \mathsf{y}_S$ is the change in the relative motion between the SpineBushing frames, and F_2^S is the generalized SpineBushing force exerted on the upper vertebra. The expressions for the components of F_2^S and $\Delta \mathsf{y}_S$ can be inferred from (17). With the help of Newton's third law, it is easy to see that an equal and opposite force and moment is exerted at the SpineBushing frame $\mathbb{S}_1$ of the lower vertebra:

$$\mathsf{F}_1^S = -\mathsf{F}_2^S. \tag{23}$$

We emphasize that using $\Delta \mathsf{y}_S$ as opposed to y_S in (22) ensures that *no forces and moments are exerted in the neutral posture.*

Implicit in (22) and (23) is the assumption that the elements of K^E are determined using the components of the forces and displacements measured in the frame of reference of the lower body, the relative rotations and increments in moments measured in the Euler and dual Euler basis respectively, and that the SpineBushing frames $\mathbb{S}_1$ and $\mathbb{S}_2$ have the same orientation as the body-fixed frames, and are situated at the landmark points used to determine the elements of K^E. If a different set of basis vectors

are used, then appropriate modifications need to be made to the expressions for F_K^S, and $\Delta \mathsf{y}_S$ to ensure compatibility with K^E.

In the interest of notational simplicity, and without any loss of generality, we will henceforth assume that these landmark points coincide with the geometric centers of the adjacent vertebrae, and this corresponds to the location of the frames $\mathbb{F}_K$. We also refer the interested reader to https://simtk.org/home/spinebushing for the software implementation of the SpineBushing element in OpenSim.

5 Application

5.1 Model details

To illustrate the issues raised in the preceding discussion, four simple models of the lumbar spine were constructed in OpenSim. All four models consisted of the vertebrae $\mathcal{L}_1$ through $\mathcal{L}_5$, with adjacent bodies connected using bushing elements (Fig. 8 and Table 1) and vertebral centers of mass situated at the vertebral geometric centers. The first, Model 1, features a bushing element with a diagonal stiffness matrix and bushing frames coincident with the joint frames while in Model 2, the bushing frames are placed at the vertebral geometric centers. Models 3 and 4 both utilize SpineBushing elements but Model 3 utilizes a diagonal experimental stiffness matrix K_D^E while Model 4 uses the full experimental stiffness matrix: $\mathsf{K}^E = \mathsf{K}_F^E$.

We estimated the elements of the stiffness matrix K_F^Ebased on the experimentally computed stiffness matrix values reported in [11] for the $\mathcal{L}_4/\mathcal{L}_5$ motion segment under 500N of preload. The components were then rearranged and scaled to align with OpenSim's coordinate system and set of units.[5] That is,

$$\mathsf{K}_F^E = \begin{bmatrix} 500000 & 0 & 0 & 0 & 0 & 11000 \\ 0 & 2500000 & 0 & 0 & 0 & -5000 \\ 0 & 0 & 500000 & -12000 & 13500 & 0 \\ 0 & 0 & -12000 & 400 & -300 & 0 \\ 0 & 0 & 13500 & -300 & 850 & 0 \\ 11000 & -5000 & 0 & 0 & 0 & 600 \end{bmatrix} \tag{24}$$

with units given in N, m and rad. Notice that this matrix has the same number of independent components and, after relabeling axes, symmetries as the stiffness matrix K in [27]. Further details on the models used, such as the geometry of the vertebral bodies are identical to those used in our earlier work [3] and we refer the interested reader to this resource for further details.

[5] The coefficients associated with their reported stiffness matrices were determined by performing highly controlled motion in one direction, measuring the ensuing forces and moments exerted at the geometric centers of the vertebrae, and then using a least-squares fit to the experimental data by the method specified in [34].

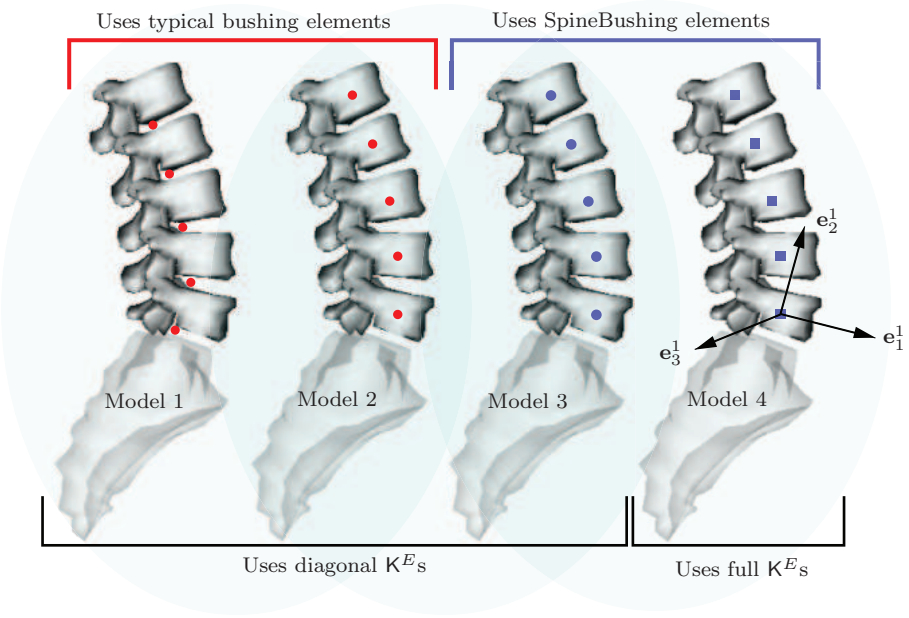

Fig. 8: *Schematic of the four models used to illustrate the application of the SpineBushing element. Model 1 and Model 2 both feature typical bushing elements and diagonal stiffness matrices but differ in the point of application of the forces and moments (red dots). Models 3 and 4 on the other hand employ SpineBushing elements and hence, exert their forces and moments at the centers of mass of the adjacent bodies but only Model 4's stiffness matrix has off-diagonal elements (circular and square points). Also shown is the set of body fixed basis vectors attached to the $\mathcal{L}_5$ vertebra. Implicit in these models is the assumption that the vertebral geometric centers are coincident with the centers of mass.*

For the case where only diagonal stiffness matrices were permitted, only the diagonal elements of the full stiffness matrix featured in (24) were used:

$$\mathsf{K}_D^E = \begin{bmatrix} 500000 & 0 & 0 & 0 & 0 & 0 \\ 0 & 2500000 & 0 & 0 & 0 & 0 \\ 0 & 0 & 500000 & 0 & 0 & 0 \\ 0 & 0 & 0 & 400 & 0 & 0 \\ 0 & 0 & 0 & 0 & 850 & 0 \\ 0 & 0 & 0 & 0 & 0 & 600 \end{bmatrix}. \tag{25}$$

For simplicity, the same stiffness matrix was used to model the joint at each level.

All four models also featured the erector spinae and rectus abdominis muscle groups. These were modeled using the Hill-type model of musculo-tendons available in the OpenSim software package [13,37,43]. The muscle parameters used are detailed in Table 2. The optimal fiber length ℓ_o^M, pennation angle at optimal fiber length α, and tendon slack length ℓ_S^T, were computed using the data and techniques detailed in

Model	Connection to Bushing Matrix	Applied At
1	$\mathsf{K}^B = \mathsf{K}^E_D$	Joint Frames
2	$\mathsf{K}^B = \mathsf{K}^E_D$	Centers of Mass
3	$\mathsf{K}^S = \mathsf{K}^E_D$	Centers of Mass
4	$\mathsf{K}^S = \mathsf{K}^E_F$	Centers of Mass

Table 1: *Summary of the four models used to illustrate the differences caused by (1) applying the stiffness matrix at the joint connecting the bodies instead of at the vertebral centers of mass, and (2) the incorporation of off-diagonal elements.*

[5]'s anatomical study, scaled to our model's geometry while the maximum isometric muscle force F_o^M were estimated from the values reported in [3].

Muscle	Maximum isometric muscle force, F_o^M (N)	Pennation angle, α (°)	Optimal fiber length, ℓ_o^M (cm)	Tendon slack length, ℓ_S^T (cm)
Rectus abdominis	700	0	21.21	1.21
Erector spinae	2500	13.9	20.00*	6.22

Table 2: *Model muscle parameters. The physiological value of ℓ_o^M for the erector spinae was actually computed to equal 7.97 cm. However, we used 20 cm instead as we found that the passive muscle forces would otherwise dominate.*

5.2 Motions

A number of different motions were examined. Pure sinusoidal translations in the anterior-posterior ($\mathbf{E}_1$) and axial ($\mathbf{E}_2$) directions were applied to Models 1 and 2 to reveal the importance of applying the bushing forces at the correct point. We also examined two separate flexion-extension motions: one involving pure flexion-extension and one coupled with axial and anterior-posterior translation. In both cases, the magnitude of the rotation of each lumbar segment was prescribed as a linear function of the total rotation which, in turn, was limited to 10° [41]. The coefficients of this linear function were determined from Wong et al.'s videofluoroscopic imaging study (cf. Figs. 10 and 11 of [42]). Table 3 summarizes the motions studied.

5.3 Muscle forces

The computed muscle control algorithm available in OpenSim was used to determine the muscle forces exerted by the rectus abdominis and erector spinae muscles in the

	$\mathcal{L}_5/\mathcal{S}_1$	$\mathcal{L}_4/\mathcal{L}_5$	$\mathcal{L}_3/\mathcal{L}_4$	$\mathcal{L}_2/\mathcal{L}_3$	$\mathcal{L}_1/\mathcal{L}_2$
	Pure Translation along $\mathbf{E}_1$				
Amplitude (mm)	0.6	0.6	0.6	0.6	0.6
	Pure Translation along $\mathbf{E}_2$				
Amplitude (mm)	0.25	0.25	0.25	0.25	0.25
	Pure Flexion-Extension				
Amplitude (°)	1.25	1.85	2.04	2.31	2.55
	Coupled Flexion-Extension				
Flexion (°)	1.25	1.85	2.04	2.31	2.55
$\mathbf{e}_1^K$ Translation (mm)	0.6	0.6	0.6	0.6	0.6
$\mathbf{e}_2^K$ Translation (mm)	0.25	0.25	0.25	0.25	0.25

Table 3: *The four sinusoidal motions used to illustrate the differences caused by (1) applying the stiffness matrix at the joint connecting the bodies instead of at the vertebral centers of mass, and (2) the incorporation of off-diagonal elements. Only small amplitude motions were tested to agree with the values used by [11] in their experimental determination of the stiffness matrices elements.*

four models specified in Section 5.1.[6] This algorithm is described in detail in [39]. Briefly, computed muscle control uses static optimization along with feedforward and feedback controls to drive the kinematic trajectory of a musculoskeletal model toward a set of desired kinematics. Since its introduction in 2003, this algorithm has been used extensively in the biomechanics community to determine, for example, the muscle forces needed to produce normal and pathological gait patterns [38], as well as to analyze muscle forces in cycling [39]. Here, we use it to quantify the effects of the bushing frame placements as well as the incorporation of off-diagonal elements on the lumbar muscle forces.

6 Results

The additional moment experienced by the vertebrae due to erroneously applying the stiffness matrix at the joint was studied by subjecting Models 1 and 3 to pure sinusoidal translations in the anterior-posterior and axial directions. The joint forces and moments exerted at the centers of mass of the upper vertebra due to the respective bushing elements below it are shown in Fig. 9. As expected, both Models 1 and 3 experienced similar forces in the axial and anterior-posterior directions but an additional moment was exerted on the vertebral bodies of Model 1. This was a consequence of applying the forces at the joint frames rather than at the centers of mass. We stress that this moment is not due to the coupling between the different degrees of freedom present in the intervertebral joint, but rather a consequence of an erroneous application of the bushing element. The implications of this are significant as the joint forces and moments directly affect the computation of muscle forces necessary to produce a given motion. Fig. 10 illustrates this for the axial translation motion: the forces exerted by

[6] It is important to note that the computed muscle forces depend on the optimization routine employed.

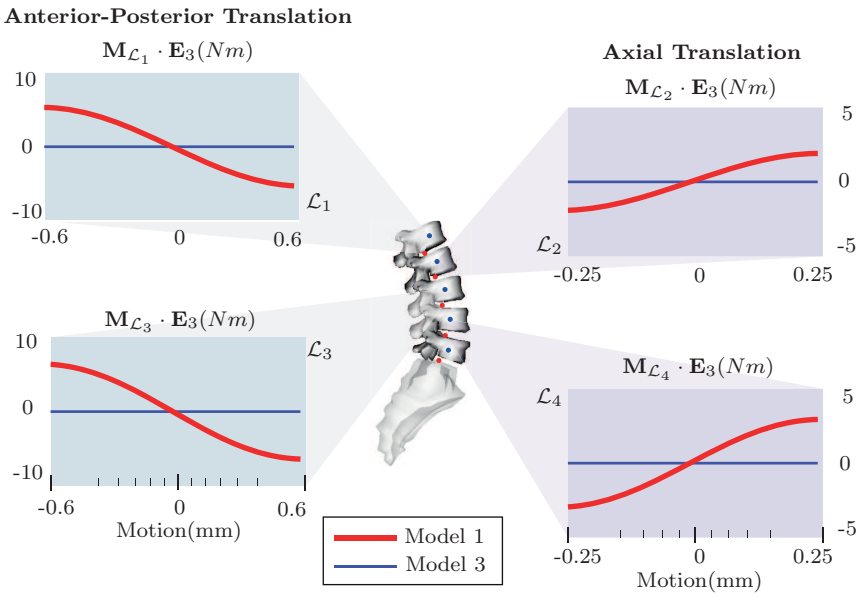

Fig. 9: *Spurious flexion-extension moment at the center of mass of the upper vertebra in Model 1 caused by the pure translations in the anterior-posterior (left) and axial (right) directions. The additional moment is due to the cross product term specified in (21). Note that the horizontal axes on the figures above are not linearly spaced due to the sinusoidal nature of the motion: the tick marks on the left (anterior-posterior translation) signify increments of 0.01mm while the tick marks for the axial-translation figures on the right signify increments of .005mm.*

the rectus abdominis are approximately similar in both models, but there is a distinct difference in the erector spinae muscle forces.

To avoid this spurious moment, one can opt to place the bushing frames at the vertebral centers of mass. Unfortunately, this introduces non-zero forces and moments in the neutral posture as detailed in Section 3 (cf. Fig. 6 and identity (19)). The magnitude of this force depends on the elements of K^B and $\mathsf{y}_{B,O}$. As the magnitude of the translational stiffnesses are typically on the order of 100,000 N/m, even an initial $\Delta\mathsf{y}_{B,O}$ of 3 cm - the typical distance between vertebral centers of mass - results in residual forces exceeding 1kN in the neutral posture! This is depicted in Fig. 11 which illustrates the additional joint forces and moments necessary to produce the anterior-posterior and axial translation kinematics described in Table 3. It is apparent that placing the bushing frames at the centers of mass instead of coincident with each other introduces additional complications due to the presence of large residual bushing forces and moments. Finally, we studied the effect of incorporating a full stiffness matrix by comparing Models 3 and 4. The off-diagonal elements of the stiffness matrix used in Model 4 exert forces and moments not present in Model 3. This results in dramatically different muscle forces as shown in Fig. 12.

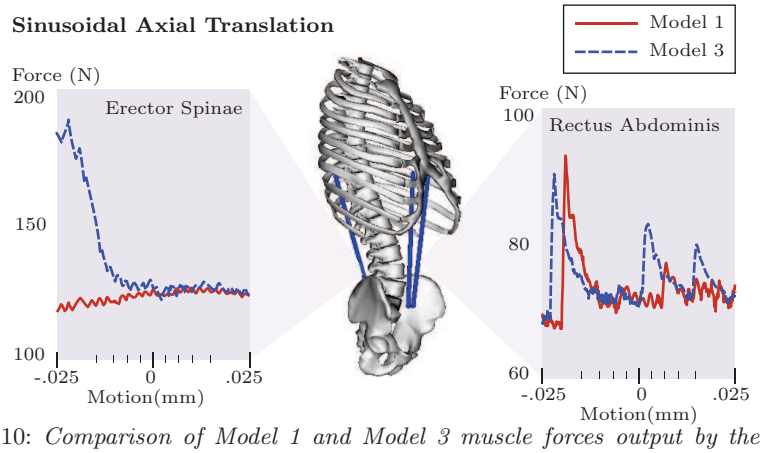

Fig. 10: *Comparison of Model 1 and Model 3 muscle forces output by the computed muscle control algorithm for the axial translation motion. Shown are the force curves for the left fascicles only as both the right and left muscle force curves were similar. Note that the horizontal axes on the figures above are not linearly spaced due to the sinusoidal nature of the motion: the tick marks shown signify increments of .005mm.*

7 Discussion and concluding remarks

Despite the simplicity of the examples used, it is apparent that adapting existing bushing elements to model the intervertebral joint can lead to numerous difficulties. Placing the bushing frames initially coincident with each other (at the joint frames) as opposed to the centers of mass appreciably altered the ensuing moments on the bodies (Figs. 9 and 10), while situating the bushing frames at the vertebral centers of mass resulted in the vertebrae experiencing tremendously large neutral forces and moments (Fig. 11). To address these two difficulties, a SpineBushing element was introduced. In contrast to typical bushing forces, the SpineBushing forces are computed using the *change* in relative motion between the SpineBushing frames. This allows the user to position the SpineBushing frames coincident with the centers of mass while simultaneously ensuring that the element exerts no forces and moments when the bodies are in the neutral posture. In addition, the SpineBushing also permits the use of the full 6×6 stiffness matrix measured experimentally, leading to a more physiologically accurate model of the load-coupling behavior of the intervertebral joint. Allowing for off-diagonal terms results in greater load sharing between the degrees of freedom, and directly affects the muscle forces necessary to generate a given motion as well as the ensuing motion patterns.

We note that the bushing element itself is an extremely useful function *when implemented correctly*. For example, in the gait model featured in [38] it is used to connect the model feet to the ground in a manner that would permit variations in ground reaction forces in a forward simulation. Others have also used the bushing element to connect musculoskeletal models feet to bicycle pedals and to connect markers to model appendages (LifeMOD, LifeModeler, Inc., San Clemente, CA). Hence, we emphasize that the issues mentioned in the present paper lie not in the bushing element itself, but in the complications that arise in using it to model the intervertebral joints of the spine.

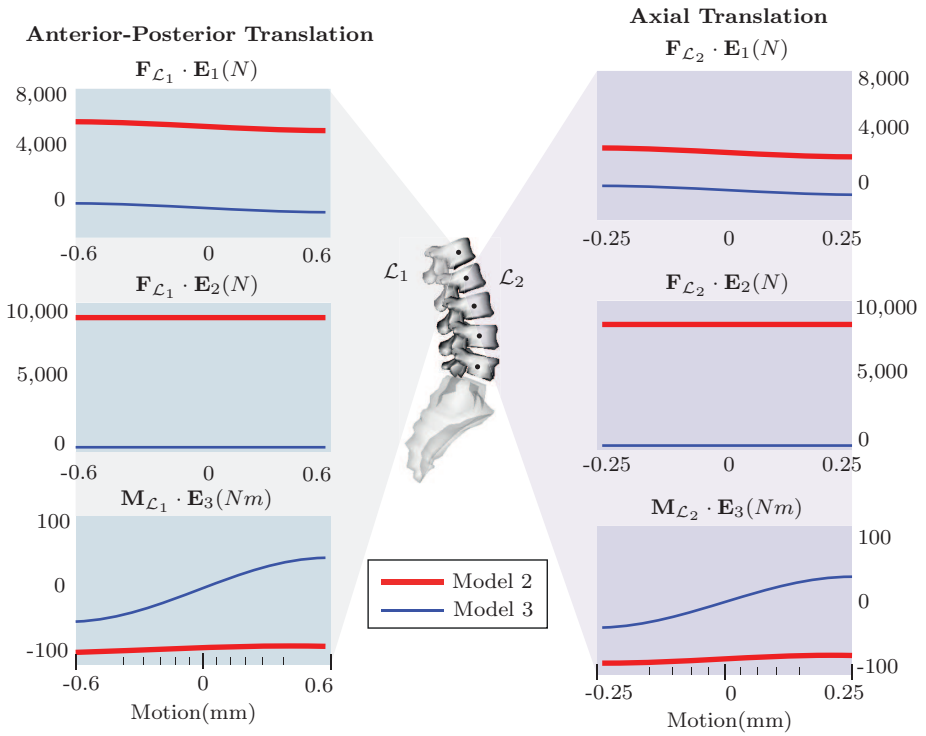

Fig. 11: *The forces and moments necessary to produce pure translations in the anterior-posterior (left) and axial (right) directions in Model 2 and Model 3 were computed using the inverse dynamics tool in OpenSim. When the bushing frames are placed at the centers of mass of the adjacent bodies, much larger forces and moments are needed in Model 2 to generate the motion patterns studied due to the residual force exerted by the traditional bushing elements when the bodies are in the neutral posture (cf. (19)). Note that the horizontal axes on the figures above are not linearly spaced due to the sinusoidal nature of the motion: the tick marks on the left (anterior-posterior translation) signify increments of 0.01mm while the tick marks for the axial-translation figures on the right signify increments of 0.005mm.*

There are a number of issues associated with the SpineBushing element that we have not explicitly addressed. Asymmetric stiffness matrices were not studied due to a lack of experimental data. Damping terms were ignored in our exposition as the applied motions were infinitesimal. Dynamically, the damping terms ensure that small perturbations to the spine are not catastrophic to the structure's stability and play an important role in protecting the joint structures from damage. Our decision to omit a discussion of damping in this work was motivated by a desire to keep the exposition as tractable as possible. However, the software implementation of the SpineBushing element does feature a 6×6 damping matrix. We also refer the interested reader to Appendix of [24] for a discussion of modeling viscous effects in models of the intervertebral disk.

Only the erector spinae and rectus abdominis muscle groups, each modeled as two fascicles with straight lines of action, were studied. Admittedly, our muscle analysis

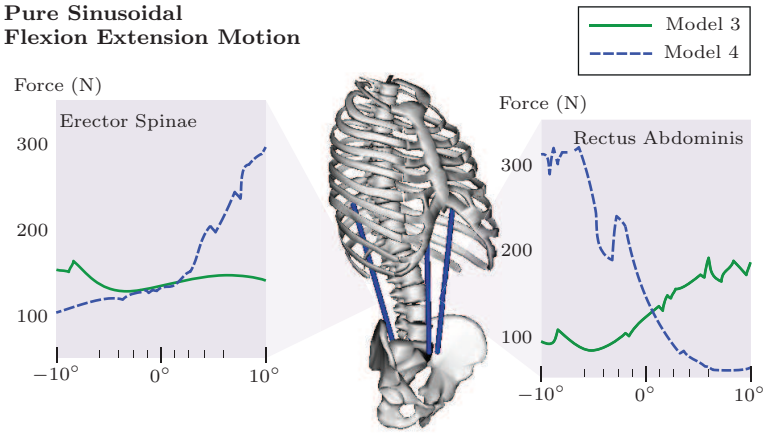

Fig. 12: *Comparison of muscle forces exerted by the erector spinae and rectus abdominis muscles of Model 3 and Model 4 for the pure flexion-extension motion. Only the forces in the left fascicle are shown as both the left and right muscle fibers produced similar force curves.Note that the horizontal axes on the figures above are not linearly spaced due to the sinusoidal nature of the motion: the tick marks shown signify increments of* 2°.

was vastly simplified. This satisfied our primary aim which was to display the changes in muscle forces due to an erroneous application of the bushing element while avoiding the high numerical load of existing models with a larger number of muscles such as the 238 fascicle model detailed in [3].

Finally, we emphasize that the purpose of this paper was to introduce the SpineBushing element and describe its proper implementation in models of the spine. The SpineBushing element proposed here is not meant to be a comprehensive model of the intervertebral joint. Rather our intention is to provide a solid and well-documented basis for future, more detailed models. Particularly useful additions include the ability for the stiffness matrix elements to be written as functions of the preload as in [22], incorporation of a damping matrix, as well as the addition of contact forces upon articulation of the vertebral facet faces.

Acknowledgements

The authors thank Professor Scott Delp and the members of the OpenSim team for their generous technical support with this software. Maurice Curtin's work was supported by Enterprise Ireland and a bursary from University College Dublin, while the four other coauthors' work was partially supported by the National Science Foundation of the United States under Grant No. CMMI 0726675.

References

1. Ambrósio, J., Verissimo, P.: Improved bushing models for general multibody systems and vehicle dynamics. Multibody System Dynamics **22**, 341–365 (2009). DOI 10.1007/s11044-009-9161-7

2. Blundell, M., Harty, D.: The Multibody Systems Approach to Vehicle Dynamics. Butterworth Heinemann, London (2004)
3. Christophy, M., Faruk Senan, N.A., Lotz, J.C., O'Reilly, O.M.: A muscloskeletal model for the lumbar spine. Biomechanics and Modeling in Mechanobiology **11**(1–2), 19–34 (2012). DOI 10.1007/s10237-011-0290-6
4. Crisco, J.J., Fujita, L., Spenciner, D.: The dynamic flexion/extension properties of the lumbar spine in vitro using a novel pendulum system. Journal of Biomechanics **40**(12), 2767–2773 (2007). DOI 10.1016/j.jbiomech.2006.12.013
5. Delp, S., Suryanarayanan, S., Murray, W., Uhlir, J., Triolo, R.: Architecture of the rectus abdominis, quadratus lumborum, and erector spinae. Journal of Biomechanics **34**(3), 371–375 (2001)
6. Delp, S.L., Anderson, F.C., Arnold, A.S., Loan, P., Habib, A., John, C.T., Guendelman, E., Thelen, D.G.: OpenSim: Open-source software to create and analyze dynamic simulations of movement. IEEE Transactions on Biomedical Engineering **54**(11), 1940–1952 (2007)
7. Ferreira, A., Silva, M.T., Levy-Melancia, J.: A multibody model of the human cervical spine for the simulation of traumatic and degenerative disorders. In: 8th World Congress on Computational Mechanics (WCCM8), Venice Italy, pp. 1–2 (2008)
8. Gardner-Morse, M.G., Laible, J.P., Stokes, I.A.F.: Incorporation of spinal flexibility measurements into finite element analysis. ASME Journal of Biomechanical Engineering **112**, 481–483 (1990)
9. Gardner-Morse, M.G., Stokes, I.A.F.: The effects of abdominal muscle coactivation on lumbar spine stability. Spine **23**(1), 86–92 (1998). DOI 10.1097/00007632-199801010-00019
10. Gardner-Morse, M.G., Stokes, I.A.F.: Physiological axial compressive preloads increase motion segment stiffness, linearity and hysteresis in all six degrees of freedom for small displacements about the neutral posture. Journal of Orthopaedic Research **21**(3), 547–552 (2003)
11. Gardner-Morse, M.G., Stokes, I.A.F.: Structural behavior of the human lumbar spinal motion segments. Journal of Biomechanics **37**(2), 205–212 (2004). DOI 10.1016/j.jbiomech.2003.10.003
12. Gercek, E., Hartmann, F., Kuhn, S., Degreif, J., Rommens, P., Rudig, L.: Dynamic angular three-dimensional measurement of multisegmental thoracolumbar motion in vivo. Spine **33**(21), 2326–2333 (2008)
13. Hill, A.: The heat of shortening and the dynamic constants of muscle. Proceedings of the Royal Society of London. Series B, Biological Sciences **126**(843), 136–195 (1938)
14. Huynh, K.T., Gibson, I., Lu, W.F., Jagdish, B.N.: Simulating dynamics of thoracolumbar spine derived from LifeMOD under haptic forces. World Academy of Science, Engineering and Technology **64**, 278–285 (2010)
15. Janevic, J., Ashton-Miller, J.A., Schultz, A.B.: Large compressive preloads decrease lumbar motion segment flexibility. Journal of Orthopaedic Research **9**(2), 228–236 (1991)
16. Kwang, T., Gibson, I., Jagdish, B.: Detailed spine modeling with LifeMOD^{TM}. In: Proceedings of the 3rd International Convention on Rehabilitation Engineering & Assistive Technology, pp. 1–5 (2009). DOI 10.1145/1592700.1592729
17. Lambrecht, J.M., Audu, M.L., Triolo, R.J., Kirsch, R.F.: Musculoskeletal model of trunk and hips for development of seated-posture-control neuroprosthesis. The Journal of Rehabilitation Research and Development **46**(4), 515–528 (2009)
18. Ledesma, R., Ma, Z.D., Hulbert, G., Wineman, A.: A nonlinear viscoelastic bushing element in multibody dynamics. Computational Mechanics **17**, 287–296 (1996). DOI 10.1007/BF00368551
19. Lee, S.H.: Biomechanical modeling and control of the human body for computer animation. Ph.D. thesis, University of California, Los Angeles (2008)
20. Lee, S.H., Eftychios Sifakis, E., Terzopoulos, D.: Comprehensive biomechanical modeling and simulation of the upper body. ACM Transactions on Graphics **28**, 1–17 (2009). DOI http://doi.acm.org/10.1145/1559755.1559756
21. van Lopik, D.W., Acar, M.: Development of a multi-body computational model of human head and neck. Proceedings of the Institution of Mechanical Engineers, Part K: Journal of Multi-Body Dynamics **221**(2), 175 – 197 (2007). DOI 10.1243/14644193JMBD84
22. Metzger, M.F., Faruk Senan, N.A., O'Reilly, O.M.: On Cartesian stiffness matrices in rigid body dynamics: an energetic perspective. Multibody System Dynamics **24**(4), 441–472 (2010). DOI 10.1007/s11044-010-9205-z
23. Monteiro, N.M.B., da Silva, M.P.T., Folgado, J.O.M.G., Melancia, J.P.L.: Structural analysis of the intervertebral discs adjacent to an interbody fusion using multibody dynamics

and finite element cosimulation. Multibody System Dynamics **25**, 245–270 (2011). DOI 10.1007/s11044-010-9226-7
24. O'Reilly, O.M., Metzger, M.F., Buckley, J.M., Moody, D.A., Lotz, J.C.: On the stiffness matrix of the intervertebral joint: Application to total disk replacement. ASME Journal of Biomechanical Engineering **131**, 081,007–1–081,007–9 (2009). DOI 10.1115/1.3148195
25. Panjabi, M., Abumi, K., Duranceau, J., Oxland, T.R.: Three-dimensional mathematical model of the human spinal structure. Journal of Biomechanics **6**, 671–680 (1973)
26. Panjabi, M.M.: Theoretical treatment of vibrations in single and multiple body suspension systems based on matrix methods. Ph.D. thesis, Chalmers University of Technology, Goteborg, Sweden. (1971)
27. Panjabi, M.M., Brand Jr., R.A., White III, A.A.: Three-dimensional flexibility and stiffness properties of the human thoracic spine. Journal of Biomechanics **9**(4), 185–192 (1976). DOI 10.1016/0021-9290(76)90003-8
28. Patwardhan, A.G., Havey, R.M., Carandang, G., Simonds, J., Voronov, L.I., Ghanayem, A.J., Meade, K.P., Gavin, T.M., Paxinos, O.: Effect of compressive follower preload on the flexion-extension response of the human lumbar spine. Journal of Orthopaedic Research **21**(3), 540–546 (2006). DOI 10.1016/S0736-0266(02)00202-4
29. Silva, M.T.: Human motion analysis using multibody dynamics and optimization tools. Ph.D. thesis, Technical University of Lisbon, Lisbon. (2003)
30. Stokes, I.A.F., Gardner-Morse, M.: Lumbar spine maximum efforts and muscle recruitment patterns predicted by a model with multijoint muscles and joints with stiffness. Journal of Biomechanics **28**(2), 173–186 (1995)
31. Stokes, I.A.F., Gardner-Morse, M.: Lumbar spinal muscle activation synergies predicted by multi-criteria cost function. Journal of Biomechanics **34**, 733–740 (2001)
32. Stokes, I.A.F., Gardner-Morse, M., Henry, S.M., Badger, G.J.: Decrease in trunk muscular response to perturbation with preactivation of lumbar spinal musculature. Spine **25**(15), 1957–1964 (2000). DOI 10.1097/00007632-200008010-00015
33. Stokes, I.A.F., Gardner-Morse, M.G.: Spinal stiffness increases with axial load: another stabilizing consequence of muscle action. Journal of Electromyography and Kinesiology **13**(4), 397–402 (2003). DOI 10.1016/S1050-6411(03)00046-4
34. Stokes, I.A.F., Gardner-Morse, M.G., Churchill, D., Laible, J.P.: Measurement of a spinal motion segment stiffness matrix. Journal of Biomechanics **35**(4), 517–521 (2002)
35. Stokes, I.A.F., Iatridis, J.C.: Basic Orthopaedic Biomechanics and Mechano-Biology, third edn., chap. Biomechanics of the Spine, pp. 529–561. Lippincott Williams & Wilkins, Philadelphia (2005). Edited by Mow, V. C. and Huiskes, R.
36. Tawackoli, W., Marco, R., Liebschner, M.A.K.: The effect of compressive axial preload on the flexibility of the thoracolumbar spine. Spine **29**(9), 988–993 (2004)
37. Thelen, D.G.: Adjustment of muscle mechanics model parameters to simulate dynamic contractions in older adults. Journal of Biomechanical Engineering **125**, 70–77 (2003)
38. Thelen, D.G., Anderson, F.: Using computed muscle control to generate forward dynamic simulations of human walking from experimental data. Journal of Biomechanical Engineering **39**, 1107 – 1115 (2006)
39. Thelen, D.G., Anderson, F., Delp, S.: Generating dynamic simulations of movement using computed muscle control. Journal of Biomechanical Engineering **36**, 321 – 328 (2003)
40. Vasavada, A.N., Li, S., Delp, S.L.: Influence of muscle morphometry and moment arms on the moment-generating capacity of human neck muscles. Spine **23**(4), 412–422 (1998)
41. White III, A.A., Panjabi, M.M.: Clinical Biomechanics of the Spine. Lippincott, Philadelphia (1978)
42. Wong, K.W.N., Luk, K.D.K., Leong, J.C.Y., Wong, S.F., Wong, K.K.Y.: Continuous dynamic spinal motion analysis. Spine **31**(4), 414–419 (2006)
43. Zajac, F.E.: Muscle and tendon: Properties, models, scaling, and application to biomechanics and motor control. Critical Reviews in Biomedical Engineering **17**(4), 359–411 (1989)
44. de Zee, M., Hansen, L., Wong, C., Rasmussen, J., Simonsen, E.B.: A generic detailed rigid-body lumbar spine model. Journal of Biomechanics **40**(6), 1219–1227 (2007). DOI 10.1016/j.jbiomech.2006.05.030